JAAS

ROYAL SOCIETY OF CHEMISTRY

PAPER

View Article Online
View Journal | View Issue

Cite this: *J. Anal. At. Spectrom.*, 2025, **40**, 1086

An improved radioisotope-based X-ray fluorescence system for the *in vivo* measurement of bone strontium†

Laura M. Bickley,[a] Eric Da Silva,[b] David R. Chettle[a] and Fiona E. McNeill *[a]

High levels of strontium can cause impaired bone growth in children, and excess mortality in animals, but at low doses there are no known toxic effects in humans. Strontium is purported to be beneficial for post-menopausal bone density loss and strontium citrate is used as a nutritional supplement by some women. This article describes development of a system to monitor bone strontium levels quickly and accurately for use in the health risk assessment of self-administered strontium supplements. Previous radioisotope-based strontium measurements take up to 30 minutes for measurements and are not portable. The new system is comprised of a silicon drift detector (SDD) with a ^{109}Cd source in a 180° backscatter geometry. Novel anthropomorphic phantoms were developed for system calibration from 3D printed PLA shells with strontium-doped hydroxyapatite cores. The system performance was investigated using two sources of different reported activity. During development, it was noted that while one ^{109}Cd source did emit an order of magnitude higher 88 keV γ-rays than the other, it did not emit an order of magnitude greater fluence of silver X-rays. This is attributed to differences in source encapsulation. This lower-than-expected X-ray fluence meant that the best minimum detectable limit (MDL) was determined to be 22 μg Sr per g Ca for a 30 minutes measurement. However, low system dead times indicated that the system was not used at maximum throughput, and it is predicted that with higher fluence silver X-ray sources, the system could achieve a minimum detectable limit of 7 μg Sr per g Ca.

Received 17th December 2024
Accepted 3rd March 2025

DOI: 10.1039/d4ja00464g

rsc.li/jaas

Introduction

Strontium (Sr) is a ubiquitous trace element present in 0.04% of the Earth's crust, which is commonly found in consumables such as produce and drinking water.[1] High levels of strontium may cause impaired bone growth in children,[2] and very high levels of Sr ingestion have been found to cause an excess in mortality in animal studies, although no known deaths from stable Sr ingestion by humans have been found.[1] Low level exposure has been shown to be non-toxic or even beneficial with one purported beneficial property of strontium being its relationship to bone mineral density (BMD). Strontium is a bone-seeking mineral, and it has been suggested that supplementing the diet with low levels of strontium could increase the BMD of humans, and potentially help treat osteoporosis. Early studies of strontium intake in animals showed an increase in new bone formation,[3–7] and a decrease in bone resorption.[4] These effects were seen in as little as four weeks, but only at higher administered doses. While these studies[3–7] did not directly measure the bone mineral density (BMD) of the animals, it was inferred that the increased bone growth would impact the bone density.

Later studies were performed on strontium ranelate, a drug initially approved for osteoporosis treatment in the European Union in 2004 (as Protelos®[8]) and Australia in 2007 (as Protos®[9]). Four large-scale clinical trials (named PREVOS,[10] STRATOS,[11] TROPOS[12] and SOTI[13]) aimed to investigate the required minimum dose for beneficial effects (PREVOS, STRATOS), and the long-term efficacy and safety of the drug (TROPOS, SOTI). These studies were able to show a clear relationship between strontium ranelate supplementation and BMD. For participants in the SOTI study, those receiving a dose of strontium ranelate of 2 g per day had a 6.8% increase in BMD averaged across three different bone sites, compared with a 1.3% decrease below the original baseline level for the placebo group.[13] Similar results were seen in the TROPOS study[12] which showed a significant increase in the BMD of women who took 2 g per day of strontium ranelate as compared with women in a placebo group. This study also showed a decrease in the number of new vertebral fractures in women receiving strontium supplementation.[12] *Post hoc* studies[14,15] on the SOTI and TROPOS groups[14] showed that for every 1% increase in BMD beyond year one, the relative risk of a new vertebral fracture dropped by an average of 3%. Rather

[a]*Department of Physics and Astronomy, McMaster University, 1280 Main Street West, Hamilton, ON, L8S 4M1, Canada. E-mail: fmcneill@mcmaster.ca*

[b]*Department of Physics, Toronto Metropolitan University, 350 Victoria Street, Toronto, ON, M5B 2K3, Canada*

† Electronic supplementary information (ESI) available. See DOI: https://doi.org/10.1039/d4ja00464g

than a single dose of 2 g per day strontium ranelate, participants in the PREVOS and STRATOS studies[16] were given a range of doses of strontium ranelate: 125 mg per day, 500 mg per day, 1 g per day or 2 g per day. The participants showing the largest increase in BMD from the original baseline were those in the 2 g per day group, with no significant effects being noted below a dose of 1 g per day. These studies also showed an increase in markers of bone formation, with levels in the 2 g per day group being significantly higher than those in the placebo group. The BMD values reported by these studies may be inflated, as studies[17,18] showed an overestimation of the BMD by 10% for every 1% increase in strontium concentration (*i.e.*, the ratio of Sr/(Sr + Ca)) in bone. This should be considered when analyzing the efficacy of supplementation.

Mild side effects were reported in these studies which included diarrhea and gastritis, although these particular studies[13–16] did not report any adverse events. However, a review by the European Medicines Agency (EMA)[19] found that those who suffered from heart disease, venous thromboembolic events, peripheral artery disease or cerebrovascular disease were at increased risk of heart attack from strontium ranelate use, and for this reason the use of the drug is now restricted in Europe. Australia[20] followed suit, restricting use of the drug in 2014.

Strontium ranelate was never approved for use in Canada, and so there are no populations of women who were prescribed the drug. However, there are Canadian women who choose to supplement their diet with strontium in the belief that it prevents or treats osteoporosis.[21,22] Compounds such as strontium citrate are available from health food stores. Canada recognizes that there may be health risks associated with strontium supplementation[23,24] and requires businesses selling supplements containing more than 4 mg strontium to attach a warning label about cardiovascular risks. Canada has also legislated a limit of strontium in drinking water of 7 mg per L per day.[25] To date, no known rigorous studies have been done on the long-term health effects of strontium citrate ingestion. A study in rodents found that strontium citrate increased the concentration of strontium in bone by a factor of 1.5 after 8 weeks.[26] Pilot studies showed that women who reported self-supplementing with strontium citrate had increasing strontium levels in bone and were often ingesting more than 100 times the daily recommended limit of strontium.[21,22] There are therefore potential populations of people in Canada who have elevated exposure to strontium, but the impact on their health is not known. Studies that compare a measured bone strontium level with the potential health risks would provide information regarding risk, allowing government to make informed decisions about the sale of these supplements.

Such studies require a method of assessing bone strontium non-invasively *in vivo*. Early work on the quantification of bone strontium *in vivo* was performed *via* animal studies[27,28] using X-ray fluorescence (XRF). Both of these early systems utilized a Si(Li) detector, and either a ^{109}Cd or ^{125}I X- and γ-ray source.[27,28] No further work was conducted on these systems beyond the initial publications, but in 2004 the technology was re-examined,[29] utilizing a Si(Li) detector, a ^{109}Cd source, 1800 s live-time measurements, and plaster of Paris (poP) phantoms. A 90° geometry was found to produce a better signal-to-noise ratio when compared to a 180° backscatter geometry. This system produced phantom based minimum detectable limits (MDL) ranging from 110 μg Sr per g Ca for low-purity phantoms to 170 μg Sr per g Ca for high purity phantoms. A re-design of the collimator in 2006 (ref. 30) further improved the MDL of the system to (44.6 ± 0.9) μg Sr per g Ca. The same Si(Li) detector was employed, but with a ^{125}I source, 1800 s live time measurements, and a 180° backscatter geometry, as the 180° geometry was easier to setup compared to the 90° geometry.[30] This MDL was further reported as being improved in 2007 to (22.9 ± 0.6) μg Sr per g Ca while using the same 1800 s live-time, geometry, detector and source and the system was applied in *in vivo* studies to measure baseline Sr levels in 22 non-supplementing subjects.[31] This same system was then used in 2008 (ref. 32) to measure strontium in tooth enamel (MDL 28 μg Sr per g Ca, measurement time 1000 s), and in 2012 (ref. 33) to measure strontium levels in human cadaver fingers [MDL (22.9 ± 0.6) μg Sr per g Ca,[34] measurement time 1800 s]. A further study used the system to investigate the difference in strontium concentrations in rats following ingestion of strontium ranelate *versus* strontium citrate[26] in 2013 although no updated MDL was reported for these rat studies. Finally, two pilot studies in 2012 (ref. 21) and 2014 (ref. 22) reported using the same system, each with an MDL of 21–23 μg Sr per g Ca[35] in phantoms, to measure the concentration of strontium in bone of volunteers who had been self-supplementing with strontium citrate. No *in vivo* MDL was able to be reported due to inherent strontium contamination of the phantoms. Other research groups developed similar systems to measure concentrations of strontium in bone,[36,37] and one study in 2017 (ref. 36) investigated the concentration of strontium in the bones of a population of children in China who had been exposed to lead.

Much of the research described above employed a measurement time of 1800 s live time. This is possibly too long for a useful clinical tool. Some groups therefore tested shorter measurements times, varying from 1 s to 1000 s.[32,33,36–39] Researchers in these two studies[36,37] were able to employ short detection times because they used an SDD detector in an X-ray tube based handheld system, that is a portable (p)XRF device. A study in human teeth[7] used shorter detection times but this does not directly translate to an indication of the required time for measurements in bone, and a study[38] aiming to develop a correction technique for soft tissue overlay was able to test the theory without a long measurement time. While most measurements in the literature are reported in terms of true times, this does not necessarily explain the clinical utility accurately. Dead times for these systems ranged from as low as 15% (ref. 21) to as high as 50%,[22] leading to actual (true or clock) measurement times of 2100 s to 2700 s. While a 40 minutes measurement is acceptable for *in vitro* studies, and experimental *in vivo* measurements, if this technology is to be translated to application outside of the laboratory, especially as a point-of-care device, then the total time of measurement should be on the same order of magnitude as other clinical procedures, such as a DXA scan. DXA scans are employed to test

the BMD of a patient over multiple bone sites in the body.[40] They typically take on the order of 5 to 20 minutes[41] in total for multiple site measurement.

This work aimed at developing an improved XRF-based *in vivo* bone strontium measurement system that could attain the required detection limits at measurement times that approach those of other point-of-care devices. We describe the development of an SDD based system employing a ^{109}Cd source, calibrated using a set of 3D printed anthropomorphic finger calibration phantoms. We discuss the accuracy of a soft tissue correction factor and show how these phantoms may create a simpler measurement system that being portable may be able to be deployed in a clinical setting.

Materials and methods

Detector and electronics

The new *in vivo* X-ray fluorescence strontium measurement system utilized a VITUS H150 Silicon Drift Detector (SDD) in an AXAS-M1 unit with an AXAS-M2 power supply and signal processing unit from Ketek GmBH Inc. fed into an ORTEC DSPEC Plus® spectrometer and computer running GammaVision© gamma spectroscopy software. The AXAS-M1 unit housed the detector, plus a reset preamplifier and the Peltier cooling system. This detector system was chosen as it can handle up to 30 000 counts per second (cps) with a rise time of 1 μs. The H150 SDD has an area of 170 mm^2 which is collimated to 143 mm^2, with an active silicon thickness of 450 μm. The detector system is encapsulated in a nickel cap with a 25 μm beryllium entrance window.

A source holder and detector cap that had been previously designed for *in vivo* measurements of iron in skin[42] was used for measurements of strontium in bone. This combination of a collimator, source holder and cap was made from aluminum with a 250 μm thick styrene window while the source holder was made of tantalum.

Excitation source

A ^{109}Cd source was used as the excitation source for the system. ^{109}Cd decays by electron capture to ^{109}Ag. An 88 keV γ-ray is emitted in approximately 4% of decays with silver (Ag) K X-rays of energy 22.2 keV and 24.9 keV being emitted in 84% and 18% of decays, respectively. The observed relative intensity of the Ag X-rays to the γ-rays is lower than these numbers indicate, as the Ag X-rays are more attenuated through the source window than the γ-rays. However, the photoelectric interaction cross section for Sr is 47.74 cm^2 g^{-1} at 22.2 keV, 35.03 cm^2 g^{-1} at 24.9 keV and 0.95 cm^2 g^{-1} at 88 keV. The combination of the higher emission intensity of the silver X-rays with the larger photoelectric cross-section means that photoelectric interactions on strontium are considerably more likely to occur with the Ag X-rays and they can be considered to be the dominant fluorescing source with contributions from the 88 keV γ-rays being considered negligible.

Two different source activities were used in this study. The sources were presumed to be identical in design having been made in the same facility: the ^{109}Cd was plated onto a 1 mm diameter circular 30 μm thick Ag plug and placed in a 3 mm × 3 mm steel capsule, with a 100 μm thick titanium entrance window. We identify this source as Source 1 which had a nominal activity of 79.82 MBq in April 2023 (down from 5.59 GBq in February 2016, calculated), while the source we identify as Source 2 had a nominal activity of 1.16 GBq in April of 2023 (down from 4.995 GBq in August 2020, calculated).

Phantoms

Three-dimensional finger phantoms were modelled in Autodesk Inventor. The fingers comprised an outer soft tissue layer which was printed from 100% infill polylactic acid (PLA) plastic (Overture). Phantoms were modelled as a hollow shell, with a length of 60 mm and inner diameter of 7.5 mm at the base of the phantom, tapering to an inner diameter of 9.7 mm at the tip of the phantom. The soft tissue layer was modelled as five thicknesses: 2 mm, 2.5 mm, 2.9 mm, 3.5 mm, and 4.0 mm. These phantom shells were then filled with strontium-doped calcium hydroxyapatite to mimic bone mineral, following the same procedure outlined previously.[43]

The calcium hydroxyapatite infill was created by adding calcium hydroxide to calcium hydrogen phosphate dibasic to achieve a Ca/P ratio of 1.67. A strontium standard solution, in the form of an ICP-OES standard solution (10 000 μg Sr per L, Ultra Scientific) was then added to reach the desired concentration. Phantoms of strontium concentration 0, 25, 50, 100, 250, 500, 750, 1000, 1250, 1500 μg Sr per g Ca were created. The components were thoroughly mixed to ensure a homogenous distribution of strontium. A setting solution of sodium phosphate dibasic (Sigma-Aldrich) was then added until a free-flowing consistency was achieved, and the mixture was poured into the 3D printed phantom shells and left to set for a week. To minimize air bubbles the shells were tapped firmly on a hard surface immediately after filling to remove any air bubbles.

A phantom with no soft tissue (hereafter referred to as a 0 mm phantom) was modelled as a cylinder with length of 60 mm and diameter 7.5 mm. These were created from a cylindrical mould with wall thickness of 2.0 mm.

The attenuation coefficient of the 3D printed plastic was measured to ensure it was a suitable soft tissue model for this X-ray energy range. While the coefficient could be calculated from the presumed composition, other studies[44] have suggested that the attenuation coefficient can vary from manufacturer to manufacturer, so empirical testing is required. A custom source holder was printed for the ^{109}Cd source, with a lead pinhole collimator. Previously printed[45] bricks of 100% infill PLA plastic with varying thicknesses (up to a total distance of 10 cm) were placed between the source and the detector and spectra acquired for 5 minutes.

The attenuation was calculated by plotting the area of the two Ag K X-ray peaks at 22.2 keV and 24.9 keV against the PLA thickness. An exponential function was fitted using Origin 2023 and the attenuation coefficients for 22.2 and 24.9 keV were calculated. These were then compared to the theoretical coefficients for soft tissue at these energies.

System geometry and phantom measurements

The detector system was set up in a 180° 'backscatter' geometry with the ^{109}Cd source mounted on the front of the detector in the tantalum source holder (Fig. 1). Finger phantoms were placed in a custom printed source holder oriented vertically and placed at an estimated distance of 2 to 3 mm from the source. The 0 mm phantom was oriented horizontally to the source. The deadtime was kept to between 2% to 5%.

Phantoms were each measured for 5 minutes and 30 minutes live time for each source resulting in a total of 4 sets of calibration measurements. The 0 μg Sr per g Ca hydroxyapatite phantoms for each tissue overlay thickness were measured 5 times, while all other hydroxyapatite phantoms were measured 3 times for each source. Between measurements each phantom was removed and replaced for the next measurement.

Peak fitting was performed using Origin 2023. A mathematical model was fitted to the spectra to extract X-ray peak areas and the Levenberg–Marquardt method of analysis was used to find the best fit. A sample spectrum from a 1500 μg Sr per g Ca strontium phantom is shown in Fig. 2. Strontium K_α and K_β X-rays and features from Compton and coherently scattered Ag X-rays (22.2 keV and 24.9 keV) are clearly observed, as is an X-ray signal from nickel in the detector.

The 14.1 keV Sr K_α X-ray, the Ni K_α X-ray, and the 22.2 keV and 24.9 keV coherently scattered Ag K X-rays from the ^{109}Cd decay were fitted using a Gaussian function with a linear background model (eqn (1) below). The 15.9 keV strontium K_β X-rays were fitted using two linked Gaussian functions on a linear background model (eqn (2) below). The Compton scatter distribution from the Ag X-rays were fitted using a Voigt function given by OriginPro 2023 on top of a complementary error function background model (eqn (3)–(5) below).

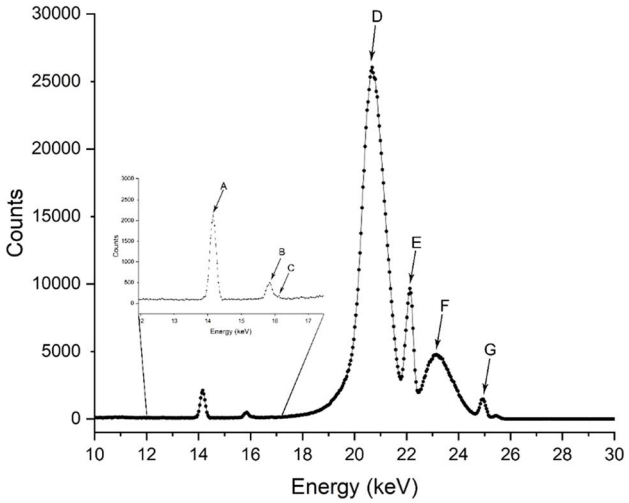

Fig. 2 An 1800 seconds live time strontium spectrum of a 1500 μg Sr per g Ca phantom, with 2 mm soft-tissue overlay thickness showing the coherently (E) and (G) and Compton scattered silver -rays (D) and (F) and an expanded view of the strontium X-rays (A)–(C). The front surface of the phantom was placed at a distance of approximately 2 mm from the ^{109}Cd source.

$$G(x) = mx + b + Ae^{-\frac{(x-\mu)^2}{2\sigma^2}} \quad (1)$$

where m and b are the slope and intercept of the background, and A, mu and sigma are the amplitude, centre and standard deviation of the Gaussian.

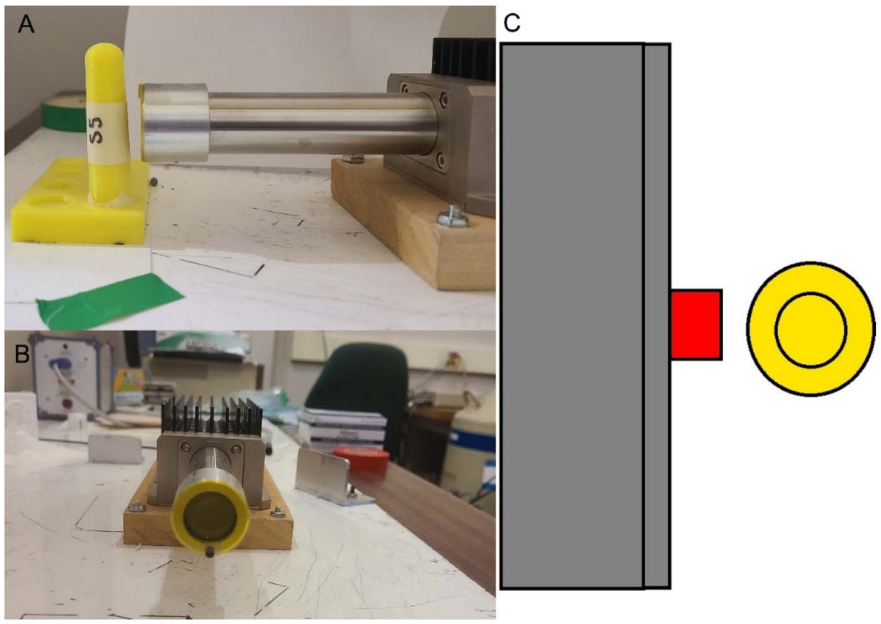

Fig. 1 A photograph showing the detector and phantom holder with phantom on the top left (A), and a head-on view of the detector in the bottom left (B). On the right (C) is a not-to-scale diagram of a top-down view of the detector showing the location of the source in the 180° backscatter geometry. Grey is the detector head, red is the tantalum source holder, and yellow is a finger phantom. Note: the source is centered when one looks at it from above (C).

$$G(x) = mx + b + A_1 e^{-\frac{(x-\mu_1)^2}{2\sigma_1^2}} + A_2 e^{-\frac{(x-\mu_2)^2}{2\sigma_2^2}} \quad (2)$$

where m and b are the slope and intercept of the background, μ_1, σ_1 and A_1 are the centre, standard deviation and amplitude of the first Gaussian, and μ_2, σ_2 and A_2 are the centre, standard deviation and amplitude of the second Gaussian.

$$y = y_0 + \int_{-\infty}^{\infty} (f_1 \times f_2)\mathrm{d}x + erfc\left((x - x_c)\Big/\left(\sqrt{2\pi}\, w_G\right)\right) \quad (3)$$

$$f_1(x) = \frac{2A}{\pi} \frac{w_L}{4(x - x_c)^2 + {w_L}^2} \quad (4)$$

$$f_2(x) = \sqrt{\frac{4\ln(2)}{\pi}} \frac{e^{-\frac{4\ln(2)}{{w_G}^2} \times x^2}}{w_G} \quad (5)$$

where x_c is, w_L is the width of the Lorentzian, w_G is the width of the Gaussian, and A is the area of the Lorentzian.

Net peak areas for the strontium K_α and K_β X-rays were plotted against phantom concentration for each tissue overlay thickness to obtain calibration lines for each finger phantom tissue overlay thickness. The MDL for each phantom thickness set was then calculated as twice the uncertainty in the zero-concentration phantom divided by the slope of the appropriate calibration line to obtain the detection limit in units of μg Sr per g Ca.

Strontium is a ubiquitous contaminant in calcium compounds and there is often an observed non-zero calibration line intercept arising from strontium in the phantom materials. The strontium concentration of potential phantom contamination was calculated by dividing the intercept of the calibration line by the slope of the given calibration line. This assumes the intercept on the calibration line arises solely from contamination and that the spectral fitting function does not introduce an artifact.

Compton thickness estimates

Strontium produces low energy X-rays that can be significantly attenuated by soft tissue. To accurately estimate strontium bone content, some method of soft tissue estimation is required. Previous studies[21,22,29,31] have employed ultrasonography to obtain estimates, but this is costly and adds a layer of complexity to the measurement. To test whether accurate

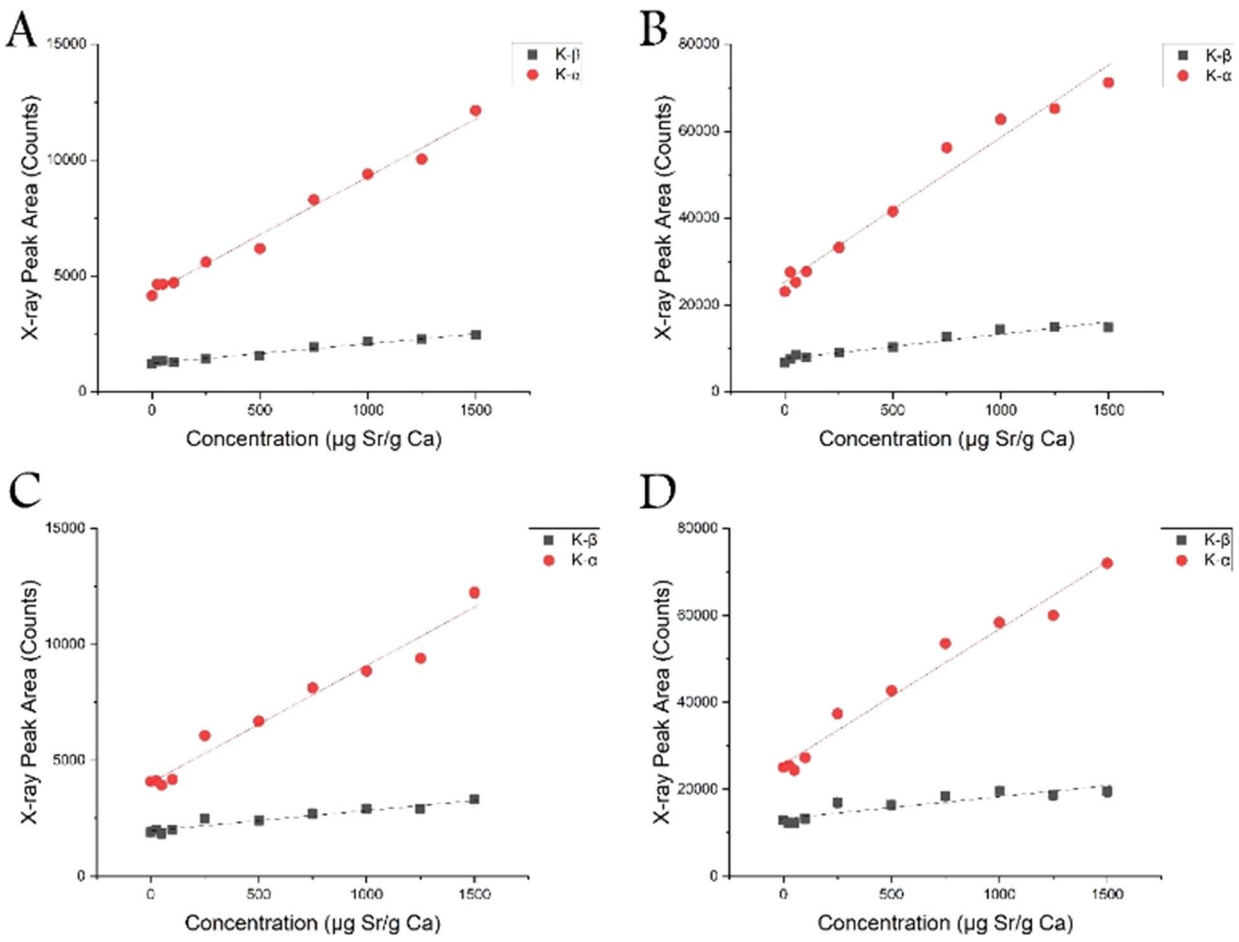

Fig. 3 Calibration lines obtained from 2 mm thick printed PLA finger phantoms for K_α X-ray area *versus* concentration (red) and K_β X-ray area *versus* concentration (black) for both sources and both measurement times. Images (A) and (B) show the 5 minutes (A) and 30 minutes (B) measurement time for Source 1, while images (C) and (D) show the 5 minutes (C) and 30 minutes (D) measurement time for Source 2. While Source 1 and 2 are reported as being a factor of 10× different in activity, this is not observed in the calibration lines.

estimates of the tissue overlay thickness could be extracted from the phantom spectra, a modified version of a published Compton thickness estimate technique[38] was implemented. In brief, a relationship between the size of the Compton scatter distribution from the 22.2 keV and 24.9 keV Ag X-rays and the soft tissue thickness was tested. This was estimated based on the net peak areas from the 1500 μg Sr per g Ca phantoms for each source and measurement time combination. This relationship was then used to estimate the soft tissue thickness, which was compared with the known value of tissue thickness of the phantom. By plotting the estimated soft tissue thickness against the known value of soft tissue thickness, the slope and significance of the relationship can be calculated, thus showing whether thicknesses could be determined reliably in unknown measurements.

Results

PLA plastic as a soft tissue surrogate

The measured mass attenuation coefficients for PLA plastic at 22.2 and 24.9 keV were 0.672 $cm^2\ g^{-1}$ and 0.579 $cm^2\ g^{-1}$ respectively. These compare extremely well to the attenuation coefficients for the NIST tabulated ICRU four component soft tissue model of 0.673 $cm^2\ g^{-1}$ and 0.565 $cm^2\ g^{-1}$. The differential attenuation through 1 cm of soft tissue *versus* through 1 cm of PLA would be 7.9% at 22.2 keV and 8.5% at 24.9 keV. At the expected tissue overlay thicknesses of soft tissue in the finger, the differences in attenuation would thus be negligible.

Calibration lines, sensitivity and MDL

Fig. 3 shows example calibration lines for both ^{109}Cd sources for counting times of 5 minutes and 30 minutes. All calibration lines are shown for the 2 mm (the thinnest PLA printed tissue overlay) thickness finger phantom. The slope of the regression of K_α X-ray peak area *versus* phantom concentration and K_β X-ray concentration *versus* phantom concentration were highly significant ($p < 0.001$, $R^2 > 0.85$) for all PLA printed phantoms. The slope of the regressions for the zero tissue overlay thickness phantoms against phantom concentration were poorer than the slopes of phantoms with tissue overlay, with the significance ranging from $p = 0.012$ to $p < 0.001$, and R^2 values ranging from 0.26 to 0.94.

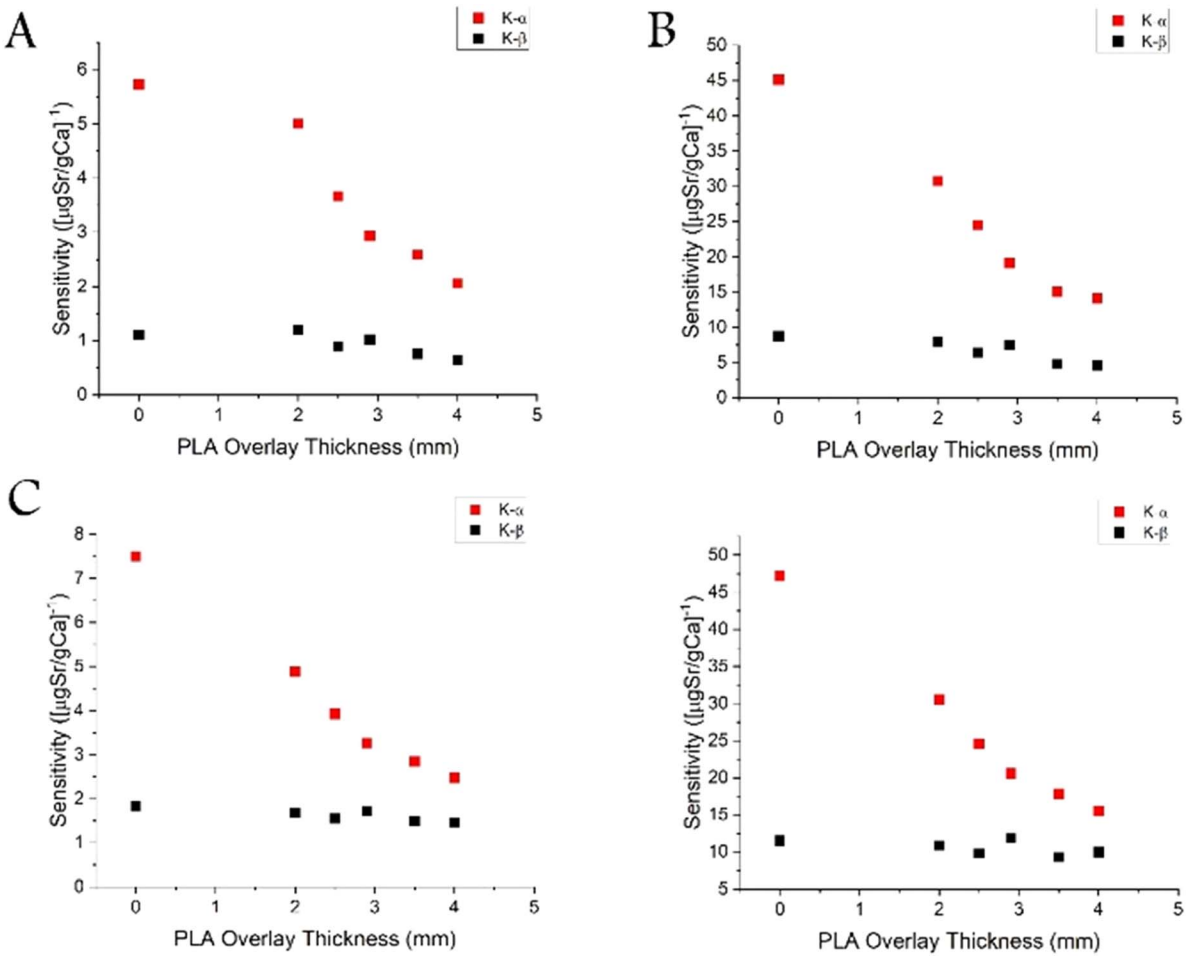

Fig. 4 The sensitivity of the detection system defined as X-ray peak area detected per μg Sr per g Ca for K_α X-ray area *versus* phantom wall thickness in mm (red) and K_β X-ray area *versus* phantom wall thickness in mm (black) for Source 1 ((A) – 5 minutes, (B) – 30 minutes) and Source 2 ((C) – 5 minutes, (D) – 30 minutes). While the two sources are reported as being a factor of 10× different in activity, this is not observed in the sensitivity signal.

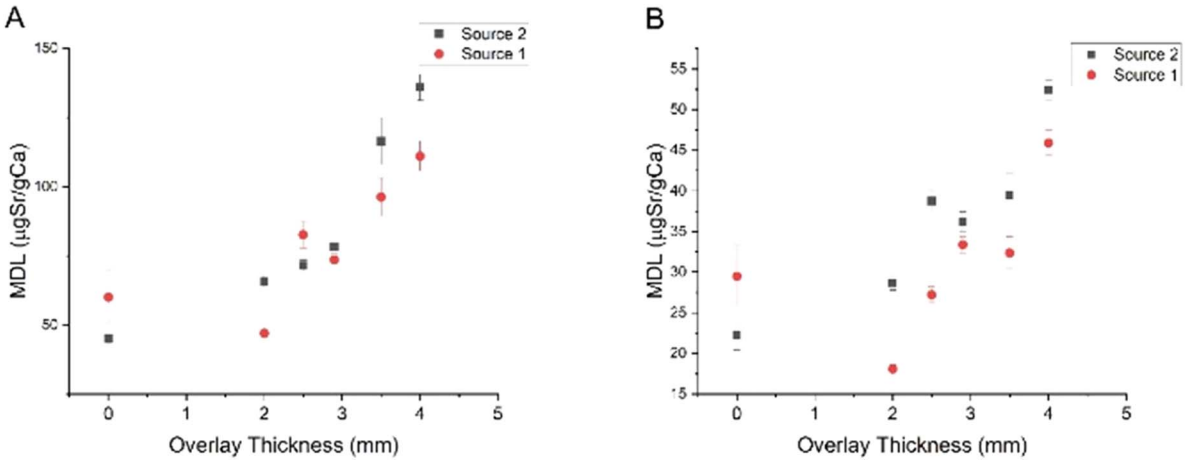

Fig. 5 The K_α X-ray based MDL for different wall thicknesses of phantoms for Source 1 and Source 2 for 5 minutes (A) and 30 minutes (B). The difference in the MDL suggests that Source 2 only emits a factor of approximately 1.8 times more silver X-rays than Source 1 despite the sources reportedly being a factor of 10 different in activity.

Fig. 4 shows the sensitivity of the system *i.e.* the measured K_α and K_β peak area counts per μg Sr per g Ca for both sources and both times. As expected, the sensitivity decreased with increasing finger phantom soft tissue thickness. Source 2 is reported by the manufacturer as being a factor of 10 times more active than Source 1. However, for the 5 minutes counts and the 30 minutes counts, the sensitivity was found to be only 25% and 10% higher, respectively.

Fig. 5 shows the MDL as determined from the K_α calibration line *versus* phantom wall thickness for both sources for 5 minutes and 30 minutes, respectively. As expected, the MDL becomes poorer with increasing phantom wall thickness. Only the K_α detection limit is shown. The K_β detection limit was calculated but was significantly poorer than the K_α detection limit in every instance. Overall, when the K_α and K_β MDLs were combined, (using an inverse variance weighted mean), it was found that the addition of the K_β information only improved the detection limit by (1.0 ± 0.2)% on average. As so little extra information was provided, further analysis focused solely on the K_α calibration slope. Table 1 shows the MDLs for the thinnest and thickest phantoms for both sources for both time intervals. The relationship between the 5 minutes and 30 minutes MDLs for each source were found to be close to the expected value of 0.41 (from $1/\sqrt{6}$). The ratio of the 30 minutes MDL to the 5 minutes MDL for Source 1 was 0.40 ± 0.03 while the ratio for Source 2 was 0.43 ± 0.03.

Phantom contamination

As can be seen in Fig. 3, all the K_α X-ray-based calibration lines had a positive intercept, and our hypothesis is that this is most likely due to strontium contamination in the calcium ingredients of the phantoms. Contamination levels were calculated for each set of calibration data by assuming that the intercepts on the calibration lines are an estimate of the contamination level in units of μg Sr per g Ca. Table 2 shows two estimates for each calibration line. The first estimate is a calculation of the mean estimate from all phantom wall thickness calibration lines for a specific source and time. The second estimate calculates an inverse variance weighted mean (IVWM) as uncertainties on estimates from individual calibration lines varied. An estimate is also calculated for each method using all data combined. Results were consistent and appear to indicate a level of contamination of approximately 800 to 850 μg Sr per g Ca.

Compton tissue thickness estimate

Table 3 shows the results of the regressions of the tissue thickness estimated using the Compton tissue technique *versus* the known thickness. As can be seen, the Compton correlation method estimate was strongly correlated with the overlying soft-tissue thickness for both sources for both time periods and the slopes were not statistically different from 1. The correlation method developed here used the known thickness estimates, so

Table 1 Minimum detectable limits for both sources for both counting times for the thinnest and thickest phantoms. The MDLs for individual sources for the different counting times change as expected. The MDL for Source 2 was expected to be approximately 3 times better than for Source 1 but is only a factor of approximately 1.8 better

Source	Time (s)	MDL (μg Sr per g Ca) 0 mm thickness	MDL (μg Sr per g Ca) 4 mm thickness
Source 1	300	60	110
Source 2	300	45	136
Source 1	1800	29	46
Source 2	1800	22	52

Table 2 Strontium contamination as estimated from calibration line intercepts for both sources for both counting periods. As the individual estimates had differences in uncertainty, an inverse variance weighted mean (IVWM) was calculated in addition to the mean

Source	Mean Sr contamination (mg Sr per g Ca)	IVWM Sr contamination (mg Sr per g Ca)
Source 1 5 minutes	0.92 ± 0.03	0.86 ± 0.03
Source 1 30 minutes	0.87 ± 0.1	0.77 ± 0.03
Source 2 5 minutes	0.79 ± 0.03	0.76 ± 0.03
Source 2 30 minutes	0.85 ± 0.04	0.82 ± 0.03
Average	0.86 ± 0.03	0.80 ± 0.01

Table 3 Regression statistics for correlation of known PLA thickness and the estimated thickness using the Compton tissue thickness technique to assess the robustness of the technique. Note that the slope value is unitless as we are plotting known thickness (mm) against calculated thickness (mm)

	Slope	R^2 of correlation	*P*-Value correlation	*Z*-Score (difference of slope from 1)	*P*-Value (two-tailed test) for *Z* score
Source 1 5 min	0.99 ± 0.10	0.957	0.00245	−0.11	0.912
Source 1 30 min	0.93 ± 0.07	0.976	0.00104	−1.00	0.353
Source 2 5 min	1.20 ± 0.12	0.958	0.00238	1.64	0.230
Source 2 30 min	1.14 ± 0.08	0.979	8.45×10^{-4}	1.71	0.087
Mean slope estimate	1.07 ± 0.09	N/A	N/A	0.780	0.435

the correlation is expected. However, we wished to assess the value and strength of the correlation to assess the robustness of the technique, by calculating forwards and backwards. The average slope from all four sets of data was 1.07 ± 0.09 and suggests that the Compton tissue technique could provide an estimate of soft tissue thickness for this measurement system, thus obviating the need for additional measurements such as ultrasonography to be employed.

Normalization to nickel signal

The solid angle subtended by the source on the phantom or finger and the solid angle subtended by the phantom or finger with the detector changes with the position of the phantom. The signal will thus vary in a clinical measurement with any patient motion. If a calibration line based on the Sr K_α X-ray measured at a fixed distance is used, this will mean measurements could potentially be inaccurate if the patient moves. A signal from nickel was observed in the spectrum. This signal arises from the detector itself[42] and has been found to be dependent on the measurement system geometry. We hypothesized that the strontium signal and the nickel system would vary in the same way and the potential for a normalization to the nickel signal was investigated.

The R^2 and *p*-values values for the strontium K_α calibration lines for both sources and both measurement times and the R^2 and *p*-values for the calibration lines with the strontium K_α X-ray signal normalized to the nickel K_α X-ray signal were examined. If we assume that the removal and replacement of phantoms between measurements could result in variation of position, then a successful normalization method should improve the linearity of the calibration lines. R^2 and *p*-values of all calibrations found that any improvement in linearity of the calibration line as a consequence of the normalization were negligible. Only 2 out of 24 Ni K_α/Sr K_α calibration lines showed improvement over the K_α X-ray signal calibration lines alone, with R^2 values improving from 0.80 to 0.84, and 0.96 to 0.97, and *p*-values improving from <0.0003 to <0.0002.

Discussion

Minimum detection limits

Previously published *in vivo* Sr measurement systems have utilized a range of detector types and sources as described earlier in this article. Table 4 presents a summary of the information with detection limits for the different systems for specific live measurement times. As can be seen, the best previously reported MDLs for a radioisotope-based system were in the range 21–23 μg Sr per g Ca[35] for an 1800 s live time measurement. The MDL obtained using source 2 in our new system is comparable, being 22 μg Sr per g Ca for an 1800 s measurement. While the MDL has not been improved, this new system does offer one significant advantage over prior radioisotope-based systems in that it is portable.

The use of an SDD was expected to attain a lower detection limit through the faster processing ability of this type of detector. However, the dead times in this ^{109}Cd system were low, in the range from 4–5%. This system did not achieve input count rates where the SDD, despite having a smaller detector surface area, could have an advantage over a Si(Li) detector. There is therefore an opportunity for improved detection limits if a source with significantly higher Ag X-ray fluence rates could be used.

The use of Source 2, a reportedly significantly higher activity ^{109}Cd source (as assessed from the 88 keV signal strength), was expected to result in an approximate factor of 10 greater Ag X-ray fluence, and thus a factor of 3 improvement in the MDL. The

Table 4 A summary of the MDLs attained for various measurement times for various K XRF systems for the *in vivo* measurement of strontium

	Fluorescing source	Acquisition time (s)	MDL (μg Sr per g Ca)
Pejovic-Milic *et al.* 2004 (ref. 29)	^{109}Cd	1800	250 (finger, *in vivo*) 560 (tibia, *in vivo*) 110 (low purity phantom) 170 (high purity phantom)
Zamburlini *et al.* 2006 (ref. 30)	^{125}I	1800	44.6 (phantom)
Zamburlini *et al.* 2007 (ref. 31)	^{125}I	1800	22.9 (finger phantom)
Heirwegh *et al.* 2012 (ref. 33)	^{125}I	1800 or 3600	22.9 (*ex vivo* finger)[18]
Moise *et al.* 2012 (ref. 21) and Moise *et al.* 2014 (ref. 22)	^{125}I	1800	21–23 (phantom)[26]
Specht *et al.* 2017 (ref. 36)	PXRF	120	1.3 (no soft-tissue equivalent) 14.5 (9 mm thickness soft-tissue equivalent)
Zhang *et al.* 2022 (ref. 37)	PXRF	120, 180, 300	5.2 (5 mm thickness soft-tissue equivalent)
This work Source 1	^{109}Cd	300	60 (0 mm) and 111 (4 mm)
This work Source 2	^{109}Cd	300	45 (0 mm) 136(4 mm)
This work Source 1	^{109}Cd	1800	29 (0 mm) and 46 (4 mm)
This work Source 2	^{109}Cd	1800	22 (0 mm) and 52 (4 mm)

MDL was thus expected to be of the order of 15 μg Sr per g Ca for a 300 s counting time and 7 μg Sr per g Ca for an 1800 s counting time. This would have been a marked improvement over the previous radioisotope-based system. This was not observed in practice. Strontium K_α X-ray signal sensitivities were only a factor of 1.8 higher for Source 2 as compared to Source 1.

Comparison of the spectra for the same phantom for the two different sources determined that the relative heights of the silver 22 keV and 24.9 keV X-rays were different between the sources. In addition, the relative size of the background above 25 keV was significantly higher in Source 2. Direct measurements of each source were made through a pinhole collimator, and it was observed that the relative heights of the 88 keV, 24.9 keV and 22 keV peaks were different (Fig. 6). This change in relative height is likely a result of differential attenuation, and so we hypothesize that the source encapsulation was slightly different. Using the changes between the 22 keV and 24.9 keV photons we estimate that source 2 has a thicker capsule that would crudely equate to approximately a 200 μm greater thickness of steel.

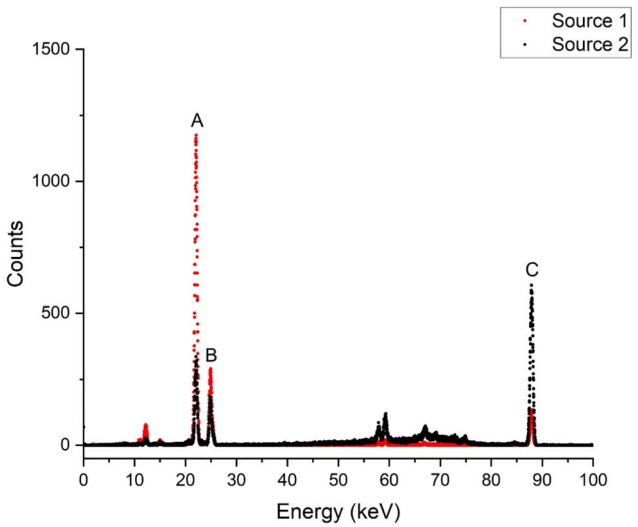

Fig. 6 Comparison of relative heights of the spectrum for two different ^{109}Cd sources: Source 1 (Red) and Source 2 (Black). Measurement time of 60 s. Peak A corresponds to the 22.2 keV Ag K_α, peak B corresponds to the 24.9 keV Ag K_β, and peak C corresponds to the 88 keV γ-ray from the decay of ^{109}Cd. Source 2 has a thicker capsule, with approximately 200 μm greater thickness of steel. The above spectrum was collected on an HPGe detector.

The small improvement in MDL with Source 2 is unexpected; however, an estimate of the MDL can be made for a higher activity source of the encapsulation type of Source 1. When Source 1 was purchased, it was a factor of 70 higher in activity than when measurements were performed. However, a 70 times greater Ag X-ray fluence would create too high a dead time to make measurements feasible. Simple calculations using a paralyzable deadtime model suggest that a source of encapsulation type 1 that is 16 times higher in activity would result in a deadtime in this system of 40 to 50%, however this could be further reduced with faster electronics. This suggests that the system could attain a MDL of 7 μg Sr per g Ca using a source of that encapsulation type for an 1800 s live time measurement, which would be a significant improvement over other radioisotope-based systems.

This MDL approaches the performance of hand-held X-ray set based systems, which use 22.2 keV Ag X-rays. While the handheld X-ray systems would still have better performance, likely due to higher incident X-ray fluence, there can be regulatory challenges (such as handheld X-ray systems being regulated by a different governing body than radioisotopes) to their use in human studies in some jurisdictions *e.g.* Ontario, Canada. For those jurisdictions, this ^{109}Cd-based SDD system would offer advantages of a better MDL than prior radioisotope systems, that is close to that of handheld X-ray systems, and attainable in a 5 minutes live counting time (10 minutes true counting time) measurement, if higher activity sources could be obtained. In addition, the doses delivered by these systems are extremely high, delivering 21 mSv to a 1 cm^2 area of skin in 120 s,[36] as opposed to our system which delivers 1.1 mSv to 0.8 cm^2 of skin.[42] The dose for handheld XRF systems can be

reduced, but at the cost of an increase in the MDL. There are no regulatory dose limits for this type of medical device in Ontario, but the occupational/environmental regulatory limit set for doses to the skin in Canada for a member of the public is 50 mSv per year over a 1 cm^2 area,[46] meaning that any handheld system would deliver 42% of this maximum annual dose permitted for a member of the public.

Phantoms

We have developed new 3D printed finger phantoms that are a better match to human tissue type and shape. The PLA outer material is a very good match to ICRU 4 component soft tissue, and the bone-mimicking matrix is calcium hydroxyapatite as in real bone. These phantoms are an improvement over previous calibration standards. However, strontium contamination in the matrix is a problem.

Previous studies determined levels of contamination for plaster of Paris phantoms of 363 μg Sr per g Ca,[35] while for the strontium doped calcium hydroxyapatite phantoms in this study, the level of contamination was determined to be (0.86 ± 0.03 mg Sr per g Ca), almost 3 times greater. This is unfortunate as it was hoped that the creation of hydroxyapatite phantoms would result in lower contamination levels as was found to be the case for calcium hydroxyapatite phantoms reported in 2008.[32] We hypothesize that the contamination difference is likely due to contamination of the reagents, as it was reported in 2008 (ref. 32) that one of the reagents ($CaCO_3$) had an inherent strontium contamination of approximately 420 μg Sr per g Ca, leading to a phantom containing 370 μg Sr per g Ca. Those researchers were able to purify the $CaCO_3$ reducing the contamination of the resulting phantom to 2 μg Sr per g Ca. We therefore suggest that future phantoms source appropriate reagents and purify the materials before use.

Compton thickness correction

It appears likely that the Compton correlation method will be able to predict the thickness of overlying soft tissue using this system allowing for selection of the appropriate calibration line. This will be a distinct advantage, as secondary methods of tissue thickness estimation will not need to be employed. This will reduce the costs and time associated with the measurement, improving its suitability for clinical use.

Normalization to the nickel signal

The normalization to the nickel signal was not found to result in any significant improvement to strontium K_α X-ray calibration lines. This may be due to careful and precise positioning of the phantoms between measurements relative to the source holder in this study. The Sr K_α X-ray calibration lines are good, and there was little room for improvement.

However, this normalization may still be useful for *in vivo* work. While it is straightforward to ensure a phantom is measured in the same position relative to the detector face in repeated measurements, this will not be possible with human participants. More importantly, with measurement times ranging from 120 s (ref. 36 and 37) to 1800 s (ref. 21, 22, 29, 30, 31 and 33) live times, there is potential for participants to move during the measurement. Any restraints would be required to be minimal and so participant motion is possible. A normalization that could help reduce the variation in the data would be advantageous and this should be explored in future work.

Conclusions

A K-XRF system for the measurement of Sr *in vivo* has been developed and tested. The system employs a silicon drift detector and a ^{109}Cd source. The system was able to achieve a best performance MDL in bare phantoms of 45 μg Sr per g Ca for a 5 minutes measurement time and a radiation dose of 0.2 mSv to the skin, and 22 μg Sr per g Ca for a 30 minutes measurement time and a radiation dose of 1.1 mSv to the skin. Use of the system with a higher activity source could result in MDLs of 11 and 7 μg Sr per g Ca for 5 minutes and 30 minutes measurements respectively. Radiation doses to the skin would increase to 3.2 mSv and 18 mSv respectively. This represents an improved performance over prior radioactive source-based systems, although handheld (p)XRF systems still perform a factor of 2 to 3 times better, but at the cost of a significantly higher skin dose to the patient.

Calibration against 3D printed PLA plastic phantoms suggests that the system can employ a Compton estimation method and thus the system would require no ultrasound measurements to be performed. This, in combination with the portability of the system, offers advantages over prior radioisotope-based systems. However, challenges with Sr contamination in phantom materials and the lack of a normalisation method to account for patient motion mean that further work is required. Finally, this is a phantom based study and physiological factors, such as the potential for contamination due to strontium excreted in sweat,[47] will need to be taken into account before the system can be tested in human studies.

Data availability

The calibration data supporting this article have been included as part of the ESI.† A ESI† data file has uploaded as part of this submission.

Author contributions

Contributions are described using CRediT for standardised descriptions: conceptualization: all four authors were involved in the development of ideas and formulation of the overarching research goals and aims. Formal analysis: performed by Bickley with oversight and advice from McNeill. Funding: McNeill and Da Silva and obtained operating funding through their Government of Canada NSERC Discovery grants. Chettle obtained capital funding for the detector system. Investigation: Bickley performed all experiments and data collection. Project administration: Bickley, Da Silva and McNeill all undertook aspects of management and coordination for the research activity planning and execution. Methodology: Bickley, Da Silva and McNeill were involved in the development and design of the

methods used in this work. Resources: Chettle, Da Silva and McNeill all provided resources *e.g.* materials and supplies, electronics, for this work. Supervision: Da Silva and McNeill undertook oversight and leadership for different aspects of this project. Validation: reproducibility of results and experiments was performed by Bickley with oversight by McNeill. Visualization: data presentation was performed by Bickley with advice from Da Silva and McNeill. Writing – original draft: Bickley wrote the original draft of this article, and McNeill and Da Silva contributed writing to subsequent drafts. Writing – review and editing: Bickley and McNeill contributed to the presentation of the published work and Chettle, Da Silva and McNeill provided critical review, commentary and revisions.

Conflicts of interest

There are no conflicts to declare.

Acknowledgements

The authors would like to acknowledge the tremendous help of Minahil Manzoor in filling the phantoms, as well as the help of Shereecia Bangura and Justin Bennett for 3D printing the phantom shells and source holders. Funding for this work was provided by the Natural Sciences and Engineering Council of Canada through Discovery Grants held by E. Da Silva and F. E. McNeill.

References

1 Strontium, *Encyclopaedia Britannica*, **https://www.britannica.com/science/strontium**, accessed January 2024.
2 Agency for Toxic Substances and Disease Registry (ATSDR), *Toxicological Profile for Strontium*, U.S. Department of Health and Human Services, Public Health Service, Atlanta, GA, 2004.
3 E. F. Ferraro, R. Carr and K. Zimmerman, *Calcif. Tissue Int.*, 1983, **35**, 258.
4 M. D. Grypnas and P. J. Marie, *Bone*, 1990, **11**, 313.
5 M. D. Grypnas, E. Hamilton, R. Cheung, Y. Tsouderos, P. Deloffre, M. Hott and P. J. Marie, *Bone*, 1996, **18**, 253.
6 P. J. Marie and M. Hott, *Metabolism*, 1986, **35**, 547.
7 S. C. Skornya, *CMAJ*, 1981, **125**, 703.
8 *Protelos|European Medicines Agency*, European Medicines Agency, May 15 2020, **https://www.ema.europa.eu/en/medicines/human/EPAR/protelos** accessed January 2024.
9 Strontium ranelate (Protos) for postmenopausal osteoporosis, NPS MedicineWise, November 1 2007, **https://www.nps.org.au/radar/articles/strontium-ranelate-protos-for-postmenopausal-osteoporosis**, accessed January 2024.
10 J. Y. Reginster, R. Deroisy, M. Dougados, I. Jupsin, J. Colette and C. Roux, *Osteoporosis Int.*, 2002, **13**, 925.
11 P. J. Meunier, D. O. Slosman, P. D. Delmas, J. L. Sebert, M. L. Brandi, C. Albanese, R. Lorenc, *et al.*, *J. Clin. Endocrinol. Metab.*, 2002, **87**, 2060.
12 J. Y. Reginster, E. Seeman, M. C. De Vernejoul, S. Adami, J. Compston, C. Phenekos, J. P. Devogelaer, M. Diaz-Curiel, A. Sawicki, S. Goemaere, O. H. Sorensen, D. Felsenberg and P. Meunier, *J. Clin. Endocrinol. Metab.*, 2005, **90**, 2816.
13 P. J. Meunier, C. Roux, E. Seeman, S. Ortolani, J. E. Badurski, T. D. Spector, J. Cannata, A. Balogh, E. M. Lemmel, S. Pors-Nielsen, R. Rizzoli, H. K. Genant and J. Y. Reginster, *N. Engl. J. Med.*, 2004, **350**(5), 459.
14 O. Bruyere, C. Roux, J. Detilleux, D. O. Slosman, T. D. Spector, P. Fardellone, K. Brixen, J. P. Devogelaer., M. Diaz-Curiel, C. Albanese, J. M. Kaufman, S. Pors-Nielsen and J. Y. Reginster, *J. Clin. Endocrinol. Metab.*, 2007, **92**, 3076.
15 O. Malaise, O. Bruyere and J. Y. Reginster, *Aging:Clin. Exp. Res.*, 2007, **19**, 330.
16 J. Y. Reginster and P. J. Meunier, *Osteoporosis Int.*, 2003, **14**, S56.
17 G. M. Blake and I. Fogelman, *J. Clin. Densitom.*, 2007, **10**, 34.
18 S. P. Nielsen, D. Slosman, O. H. Sorensen, B. Basse-Cathlinat, P. De Cassin, C. Roux and P. J. Meunier, *J. Clin. Densitom.*, 1999, **2**, 371.
19 *Protelos and osseor – referral|European Medicines Agency*, European Medicines Agency, September 19 2014, **https://www.ema.europa.eu/en/medicines/human/referrals/protelos-osseor**, accessed January 2024.
20 Black-box warning for strontium ranelate (Protos) added to Product Information, NPS Medicine Wise, December 1 2014, **https://www.nps.org.au/radar/articles/black-box-warning-for-strontium-ranelate-protos-added-to-product-information**, **https://www.nps.org.au/radar/articles/strontium-ranelate-protos-for-postmenopausal-osteoporosis**, accessed January 2024.
21 H. Moise, J. D. Adachi, D. R. Chettle and A. Pejovic-Milic, *Bone*, 2012, **51**, 93.
22 H. Moise, D. R. Chettle and A. Pejovic-Milic, *Bone*, 2014, **61**, 48.
23 *Summary Safety Review – Strontium – Risk of Heart and Circulatory Side Effects*, Government of Canada, October 22 2015, **https://www.canada.ca/en/health-canada/services/drugs-health-products/medeffect-canada/safety-reviews/summary-safety-review-strontium-risk-heart-circulatory.html**, accessed January 2024.
24 *Strontium health products: New Restrictions to address possible heart and circulatory-related risks*, Health Canada, October 22 2015, **https://recalls-rappels.canada.ca/en/alert-recall/strontium-health-products-new-restrictions-address-possible-heart-and-circulatory**, accessed January 2024.
25 *Strontium in drinking water – Guideline Technical Document for Public Consultation*, Health Canada, July 20 2018, **https://www.canada.ca/en/health-canada/programs/consultation-strontium-drinking-water/document.html**, accessed January 2024.
26 G. R. Wohl, D. R. Chettle, A. Pejovic-Milic, C. Druchok, C. E. Webber, J. D. Adachi and K. Beattie, *Bone*, 2013, **52**, 63.
27 R. E. Snyder and D. C. Secord, *Phys. Med. Biol.*, 1982, **27**, 515.
28 L. Wielpolski, D. Vartsky, S. Yasumura and S. H. Cohn, *Adv. X Ray Anal.*, 1982, **26**, 415.

29 A. Pejovic-Milic, I. M. Stronach, J. Gyorffy, C. E. Webber and D. R. Chettle, *Med. Phys.*, 2004, **31**, 528.
30 M. Zamburlini, A. Pejovic-Milic and D. R. Chettle, *J. Radioanal. Nucl. Chem.*, 2006, **269**, 625.
31 M. Zamburlini, A. Pejovic-Milic, D. R. Chettle, C. E. Webber and J. Gyorffy, *Phys. Med. Biol.*, 2007, **52**, 2107.
32 E. Da Silva, A. Pejovic-Milic and D. V. Heyd, *J. Anal. At. Spectrom.*, 2008, **23**, 527.
33 C. M. Heirwegh, D. R. Chettle and A. Pejovic-Milic, *Med. Phys.*, 2012, **39**, 832.
34 C. M. Heirwegh, M.Sc thesis, McMaster University, 2008.
35 H. Moise, PhD thesis, McMaster University, 2008.
36 A. J. Specht, F. Mostafaei, Y. Lin, J. Xu and L. H. Nie, *Appl. Spectrosc.*, 2017, **71**, 1962.
37 X. Zhang, E. M. Wells, A. J. Specht, M. G. Weisskopf, J. Weuve and L. H. Nie, *J. Trace Elem. Med. Biol.*, 2022, **74**, 127077.
38 J. Gevaert and D. R. Chettle, *X-Ray Spectrom.*, 2019, **48**, 443.
39 E. Da Silva, G. Mankovskii, B. Kirkham, J. Groves, M. Gherase, D. E. B. Fleming and A. Pejović-Milić, *Adv. X-Ray Anal.*, 2018, **61**, 116.
40 Bone Density Scan, Mount Sinai Hospital, **https://www.mountsinai.on.ca/care/me/bone-density-scan**, accessed January 2024.
41 Bone density scan, Canadian Cancer Society, **https://cancer.ca/en/treatments/tests-and-procedures/bone-density-scan**, accessed January 2024.
42 S. U. K. Bangash, F. E. McNeill, M. J. Farquarson and D. R. Chettle, *Biomedical Physics & Engineering Express (BPEX)*, 2022, **8**, 065034.
43 E. Da Silva, B. Kirkham, D. V. Heyd and A. Pejovic-Milic, *Anal. Chem.*, 2013, **85**, 9189.
44 J. Solc, T. Vrba and L. Burianova, *J. Instrum.*, 2018, **13**, P09018.
45 R. C. Bider, B. Sheehan, N. Bock and F. E. McNeill, *Biomedical Physics & Engineering Express (BPEX)*, 2024, **10**, 035027.
46 Canadian Nuclear Safety Commission, Radiation Protection Regulations SOR/2000-203, May 29 2024, **https://laws-lois.justice.gc.ca/eng/regulations/sor-2000-203/page-2.html#h-656867**.
47 S. P. Nielsen, The biological role of strontium, *Bone*, 2004, **35**(3), 583–588.